Article:
Huang, L, Robertson, ID, Wu, W et al. (1 more author) (2013) Substrate integrated waveguide filters with broadside-coupled complementary split ring resonators. IET Microwaves, Antennas and Propagation, 7 (10). 795 - 801. ISSN 1751-8725

https://doi.org/10.1049/iet-map.2013.0117

Substrate Integrated Waveguide Filters with Broadside-Coupled Complementary Split Ring Resonators

Liwen Huang[1], Ian D. Robertson[1*], Weiwei Wu[2] and Naichang Yuan[2]

[1] School of Electronic and Electrical Engineering, University of Leeds, Leeds, LS2 9JT, UK

[2] School of Electrical and Electronic Engineering, National University of Defense Technology, Chansha, 410073, China.

*Corresponding author: I.D.Robertson@leeds.ac.uk

Abstract— Four designs of substrate integrated waveguide (SIW) filter employing integrated broadside-coupled complementary split-ring resonators (BC-CSRR) are compared. By changing the orientation rings, four types of SIW unit cell are proposed and investigated and it is shown that, for one particular topology, two poles and two zeroes can be realised with a single unit cell. Bandpass filters based on the proposed resonators coupled by evanescent-mode SIW sections have been fabricated and tested. The proposed filters have the advantages of compact size, high selectivity, and ease of integration.

Index Terms—microwave filters, microwave integrated circuits, waveguides, metamaterials.

1. Introduction

Recently, substrate integrated waveguide (SIW) incorporating electromagnetic bandgap structures such as the split ring resonator (SRR) and complementary split ring resonator (CSRR) have been widely investigated for the design of miniature filters [1, 2]. There are various types of SRR and CSRR, including the classic edge-coupled split-ring resonator (EC-SRR), proposed by Pendry et al. [3], the broadside-coupled SRR (BC-SRR) [4], the edge-coupled complementary split-ring resonator (EC-ESRR)[5], and the broadside-coupled complementary split-ring resonator (BC-CSRR) [6]. Research has been reported on both modelling [7, 8] and the application to the design of miniaturized components such as filters and antennas [9-12]. The SIW combined with a pair of EC-CSRRs was reported in [11]. It is shown that different frequency responses can be obtained when the orientations of the EC-CSRRs are varied. The effect of the variation of the orientation of the EC-CSRRs on the frequency responses was investigated and the equivalent circuit models were derived. The SIW using the broadside-coupled complementary split-ring resonator (BC-CSRR) was reported in . A pair of BC-CSRRs was integrated into the SIW to form a miniaturized resonator unit cell and the resonator unit cell was applied in the design of compact filters. In this paper, with a similar method for the analysis of SIW with EC-CSRR pairs shown in [11], novel unit cells of the SIW loaded by BC-CSRR pairs are proposed and investigated. It is demonstrated that by changing the orientations of the top lay rings of BC-CSRRs, four distinct types of resonator can be realised. By comparing these, a structure is found that produces two poles and two zeros from a single unit cell, giving significant potential for the realisation of compact filters in SIW technology. Moreover, since the physical size of the BC-CSRR can be significantly reduced just by using a thin dielectric substrate

[6], the proposed filters also have even greater potential to achieve a more compact size in comparison to their counterparts with EC-CSRRs.

2. Type I Structure

The layout of the SIW structure with a pair of BC-CSRRs in the orientation originally proposed in [6], hereafter referred to as the Type I structure, is shown in Fig. 1(a)-(c). A pair of identical BC-CSRRs is etched on the SIW top and bottom broadwalls, with the resonators aligned side by side but at 180° to one another. A microstrip feed line is used to excite the SIW, with an inset transition used to get a better match. Since the electric field of the dominant mode within the SIW is orthogonal to the top and bottom surfaces, the CSRRs are properly excited [2].

The equivalent circuit of EC-CSRR resonators has been investigated in [11]. Here, through similar analysis, the proposed unit cell can be modelled with a simplified equivalent circuit within a limited frequency range. As shown in Fig. 1(d), the metallic vias of the SIW are modelled as L_v; the BC-CSRR pair is modelled by means of the shunt-connected resonator composed of the capacitance C_b and the inductance L_b; L_c denotes the inductive coupling which is mainly through the split of the ring between the SIW and the BC-CSRRs; C_c represents the capacitive coupling which is mainly realized by the slot coupling between the SIW and the BC-CSRRs.

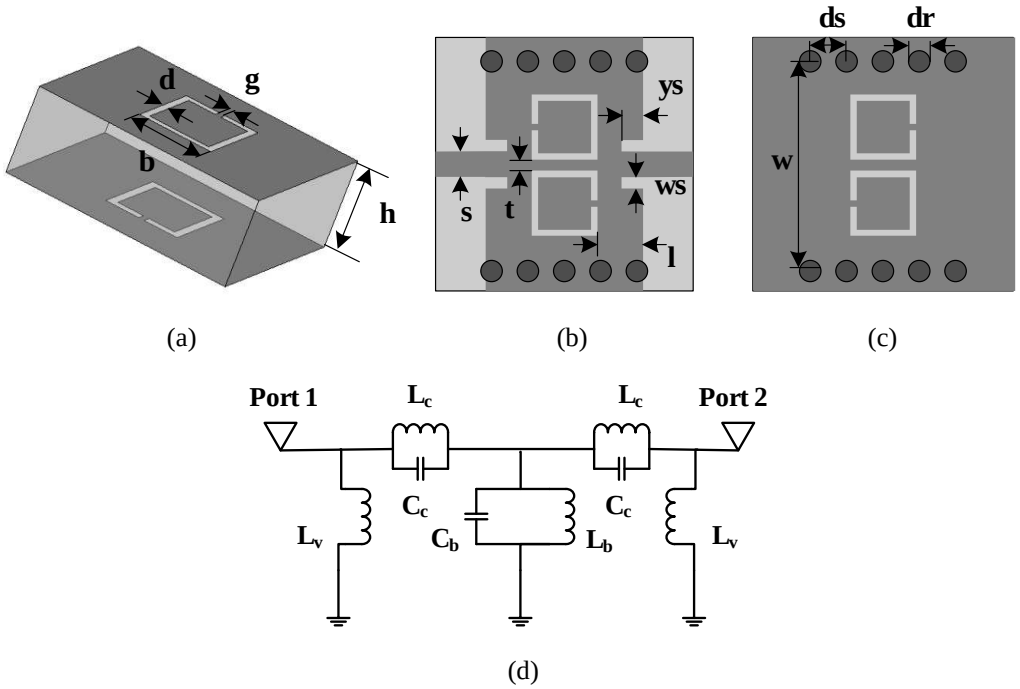

Fig. 1. (a) Configuration of the BC-CSRR. (b) Top view of the configuration of the type I unit cell of the BC-CSRR pair. (c) Bottom view[6]. (d) Equivalent circuit model. Gray shading represents the metallization.

To get the values of the equivalent circuit model of the proposed unit cell, the values of the equivalent capacitance (C) and inductance (L) of the corresponding BC-SRR can be obtained with the method shown in [7] firstly; since the BC-CSRR can be viewed as the negative image of the BC-SRR, the parameters of the LC circuit model of the BC-CSRR can then be approximated from the duality by $C_b = 4(\varepsilon/\mu)L$ and $L_b = C/(4(\varepsilon/\mu))$, where ε and μ are the permittivity and permeability of the dielectric substrate, respectively. The values of other electric parameters, L_v, L_c and C_c can be approximated by using the method presented in ref. [13]. After determining the initial parameters of the BC-CSRR, the accurate values of the equivalent circuit model of the SIW BC-CSRR unit cell can then be achieved by carrying out the simulation and optimization with the Ansoft Designer software.

An example of the unit cell of the SIW with the BC-CSRR pair was designed and investigated, with the dielectric constant of the substrate $\varepsilon_r = 2.65$ and the width of the waveguide, w, set to 12.5 mm to achieve a nominal waveguide cutoff frequency of 8.15 GHz. The HFSS^{TM} and circuit model simulated frequency responses of the SIW BC-CSRR unit cell are depicted in Fig. 2(a) (with the dimensions of the unit cell and lumped-element values of the circuit model shown in the caption). Good agreement has been achieved between the HFSS and circuit model simulations. A passband with a centre frequency of 5.61 GHz is observed. It is shown that the resonant frequency of the SIW BC-CSRR element is clearly well below the cutoff frequency of the original SIW.

To better understand the response of the proposed unit cell, we derive the dispersion relation of the equivalent circuit (see Fig. 1(d)) from classical circuit theory [14]. For simplicity, the vias, denoted by L_s, are not taken into consideration. The series impedances Z_s and shunt impedances Z_p are then given by:

$$Z_s = \frac{j\omega L_c}{1-\omega^2/\omega_1^2} \tag{1}$$

$$Z_p = \frac{j\omega L_b}{1-\omega^2/\omega_0^2} \tag{2}$$

where $\omega_1^2 = 1/(L_cC_c)$, $\omega_0^2 = 1/(L_bC_b)$. The dispersion relation can then be calculated by:

$$\cos\phi = \cos(\beta l) = 1 + \frac{Z_s}{Z_p} = 1 + \frac{L_c\left(1-\omega^2/\omega_0^2\right)}{L_b\left(1-\omega^2/\omega_1^2\right)} \tag{3}$$

Wave propagation is expected in the region where β is real. By inserting the values of the lumped elements in the caption of Fig. 2 into (1), (2) and (3), the relation between β and ω is obtained. As shown in Fig. 2(b), wave propagation is allowed between 5.03 GHz to 5.78 GHz, which agrees well with the simulated passband in Fig. 2(a). On the other hand, it is noted that, in the region between 5.03 GHz to 5.78 GHz, β increases with frequency, which means forward wave propagation. This can also be explained from the perspective of an effective medium filling the SIW. A waveguide filled with electric dipoles, namely metallic rods, has been investigated using an anisotropic electric plasma approach in [15]. Through a similar analysis, the SIW with BC-CSRRs can also be considered as an equivalent rectangular waveguide filled with an anisotropic electric plasma with the

relative permeability μ_r = 1. From [15], the dispersion relation for the fundamental mode can then be approximated by:

$$\beta^2 = -\gamma^2 = k^2 \frac{\varepsilon}{\varepsilon_0} - k_x^2 = k^2 \frac{\varepsilon}{\varepsilon_0} - \left(\frac{\pi}{W_{eff}}\right)^2 \tag{4}$$

where $k^2 = \omega^2 \mu_0 \varepsilon_0$, W_{eff} is the equivalent width of the SIW. The wave propagates at the frequencies where $\varepsilon > \varepsilon_0(\pi/(k\,W_{eff}))^2$. On the other hand, it can be seen that it is a forward wave, i.e., $d\beta/d\omega > 0$, which follows from Foster's theorem $d\varepsilon/d\omega > 0$ [16].

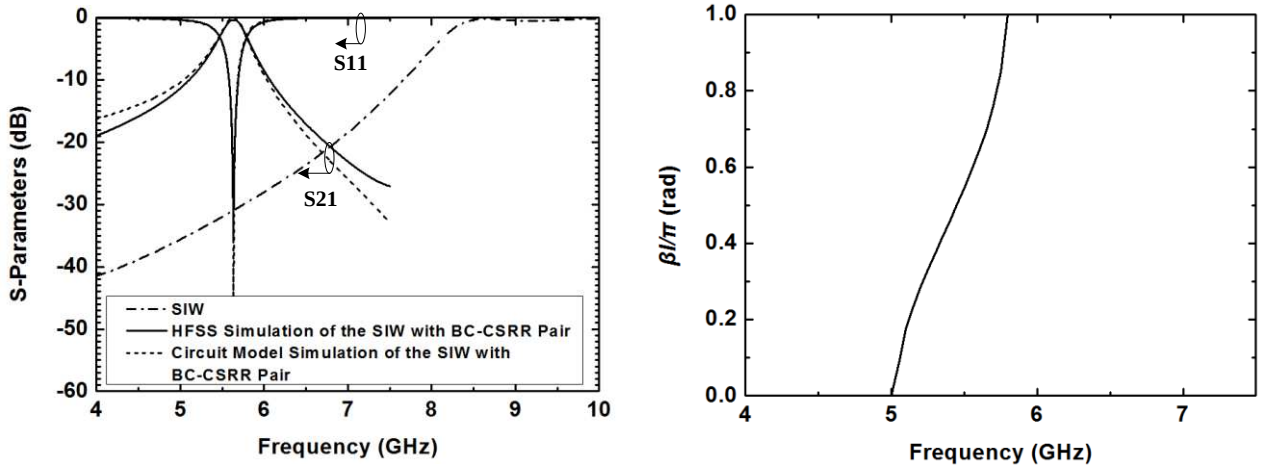

(a) (b)

Fig. 2. (a) HFSS and circuit model simulated frequency response of the standard SIW and the type I unit cell (with parameters h = 1 mm, b = 3.9 mm, g = 0.3 mm, d = 0.34 mm, t = 0.5 mm, w = 12 mm, s = 2.65 mm, ws= 0.5 mm, ys = 1.5 mm, l = 2.5 mm, dr = 1.2 mm, ds = 2.2 mm, L_v = 2.5 nH, L_c = 1.88 nH, C_c = 0.16 pF, L_b = 0.5 nH, C_b = 2 pF). (b)Theoretical dispersion relation for the type I unit cell.

3. Type II, III and IV unit cells

CSRRs exhibit different transmission responses when the orientation is altered [17]. This has been illustrated in [11], where the SIW with EC-CSRRs are investigated and the effect of changing the orientation of the EC-CSRRs on the frequency responses is analyzed. With a similar method, the proposed SIW BC-CSRR resonator structure is further investigated by varying the orientation of the BC-CSRRs. However, it should be noted that, since the coupling and the distribution of the electromagnetic fields of BC-CSRRs are different from EC-CSRRs, the influence of the orientations of the BC-CSRR on the frequency response may be also different from that of the EC-CSRR shown in [11]. In addition, unlike the structures which are proposed by varying the orientations of the whole EC-CSRRs in ref [11], here, only the orientations of the top layer rings of the BC-CSRRs are changed.

Fig. 3 shows the configuration of three types of SIW BC-CSRR resonator pairs with different orientations for the top layer rings compared to the type I unit cell (see Fig. 1). Fig. 3(a) presents the Type II unit cell, where the rings on the top are now aligned face-to-face, while the rings on the lower broadwall have not changed orientation but are now united along one edge to enhance the capacitive coupling. In the Type III structure, as shown in Fig. 3(b), the rings on the top surface have been flipped so that the slits now align with the corresponding ring on the bottom. Finally, the Type IV structure, as shown in Fig. 3(c), uses top-side rings that are back-to-back. Again, the rings on the bottom are unified along a common side.

The transmission responses of the three types of unit cells simulated using HFSS™ are plotted in Fig. 4. It can be seen that, compared with the Type I element (see Fig.1), good filtering responses with broader bandwidth have been achieved for the last three types, which indicates stronger effective coupling between the two modified BC-CSRRs. On the other hand, compared with the second and third structures which have transmission zeros only in the upper stopband (see Figs. 4(a), (b)), the Type IV exhibits a transmission zero in both the upper and lower stopband (see Fig. 4(c)), thus showing it has excellent potential for realizing miniature filters with good selectivity.

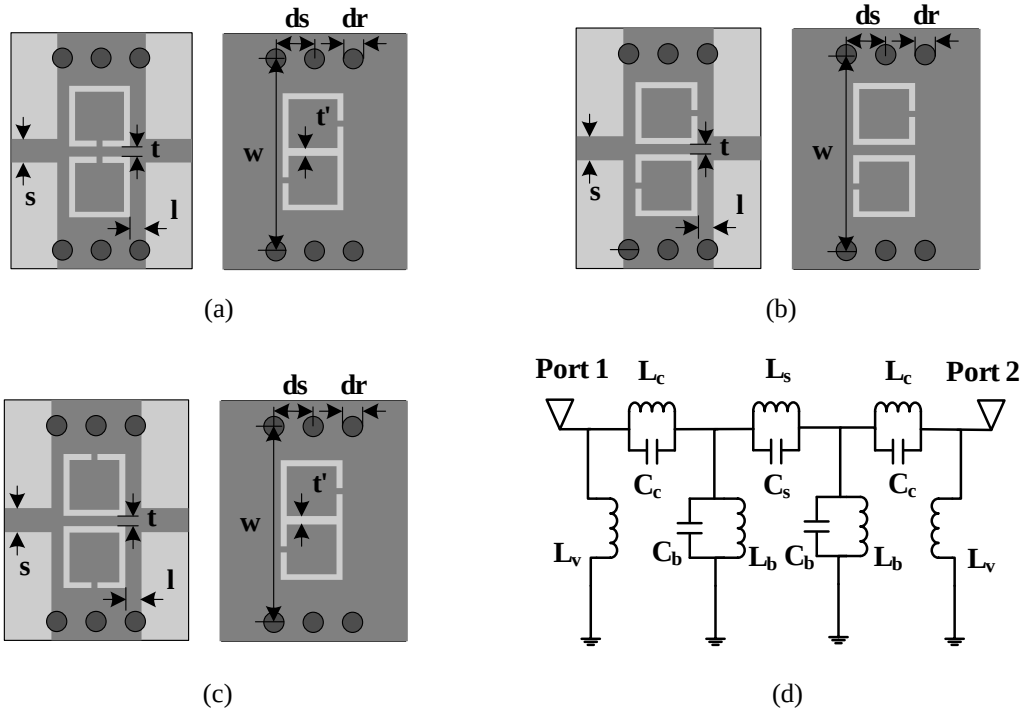

Fig.3. (a) Layout of the type II unit cell of the BC-CSRR resonator pair. (b) Layout of the type III unit cell. (c) Layout of the type IV unit cell.(d) Equivalent circuit model for type II, type III and type IV unit cells.

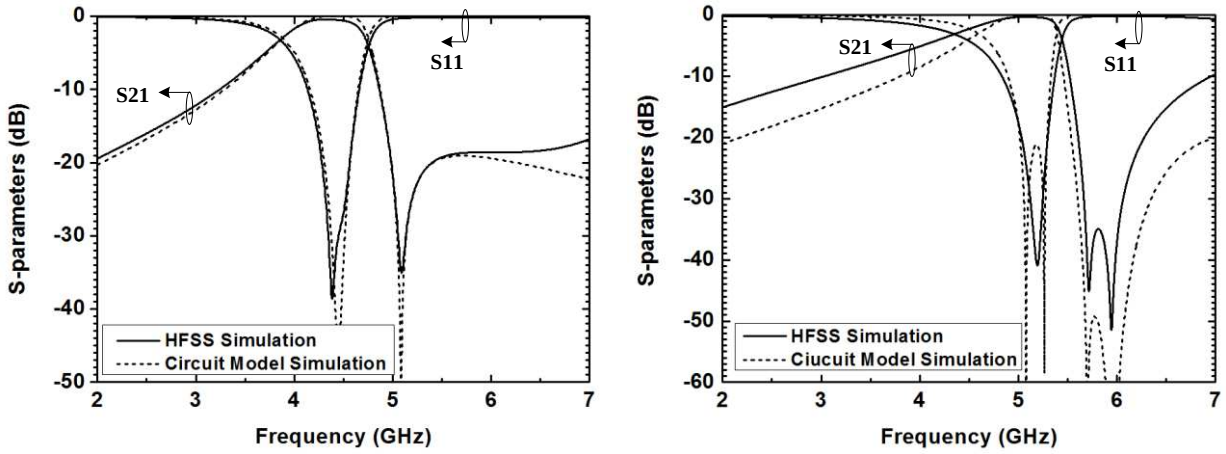

(a)

(b)

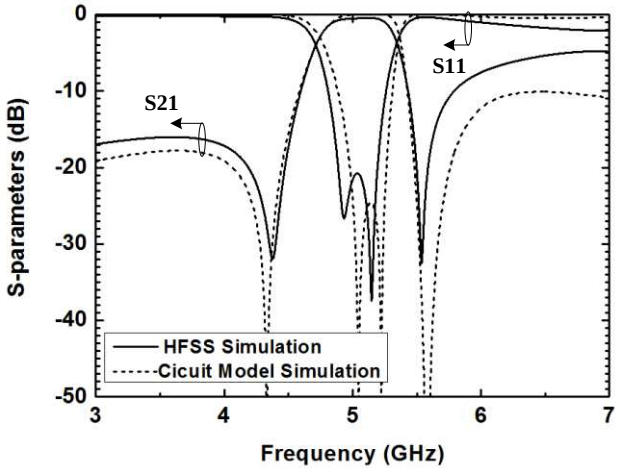

(c)

Fig.4. HFSS and circuit model simulated frequency responses of the: (a) type II unit cell, (b) type III unit cell and (c) type IV unit cell. The parameters for the type II unit cell are: ε_r = 3.48, h = 0.762 mm, b = 3.9 mm, g = 0.3 mm, d = 0.34 mm, w = 12.5 mm, s = 1.68 mm, l = 0.5 mm, dr = 1.2 mm, ds = 2.2 mm, t = 0.75 mm, and $t^{'}$ = 0.33 mm; for type III, part of the parameters are revised as t = 1.3 mm, others are the same; for type IV, part of the parameters are revised as t = 1.1 mm and $t^{'}$ = 0.38 mm, others are the same.

Table 1. Lumped-element values of the circuit model of the Type II, III and IV unit cells.

	L_v (nH)	L_c (nH)	C_c (pF)	L_s (nH)	C_s (pF)	L_b (nH)	C_b (pF)
type Ⅱ	3.6	0.35	0.65	0.49	2	0.595	2.9
type Ⅲ	4.2	0.3	2.38	0.668	1.147	0.597	2.15
type Ⅳ	4	0.18	4. 52	1	1.35	0.6	1.81

To further investigate the transmission characteristics of the Type II, III and IV unit cells, the equivalent circuit model has been derived and investigated through analysis similar to that employed in the equivalent circuit model of the type I unit cell (see Fig. 1(d)). As shown in Fig. 3(d), the metallic vias of the SIW are again

modelled as L_v. L_c denotes the inductive coupling that is mainly through the split of the ring between the SIW and the CSRRs. C_c represents the capacitive coupling that is mainly realized by the slot coupling between the SIW and the CSRRs. The modified BC-CSRR is modelled by means of the shunt-connected resonator with the capacitance C_b and the inductance L_b. However, compared with the equivalent circuit model of the first type, in terms of the last three types, the mutual coupling between resonators should be taken into account. The coupling mechanisms for the SRRs have been investigated in [18]. Here, the coupling between modified BC-CSRRs is considered as a combination of electric and magnetic types, described by C_s and L_s, respectively. The values of the equivalent circuit model of these three new unit cells can be obtained following similar procedures to the type I unit cell.

The simulated frequency responses of the three new unit cells from the equivalent circuit model and the HFSS™ are presented in Fig. 4 (with the values of the lumped elements depicted in Table 1). As shown in Fig. 4(a), for the type II unit cell, a transmission zero is introduced above the passband. This is due to the mutual coupling between the modified BC-CSRRs, denoted by C_s and L_s in the circuit model. At the frequency where the admittance of the branch is null, the branch opens and the signal propagation is suppressed, leading to a transmission zero at:

$$f_{z1} = \frac{1}{2\pi\sqrt{L_s C_s}} \tag{6}$$

The type III unit cell introduces an additional transmission zero which is above the first transmission zero. This additional transmission zero is created by the coupling between the SIW and the modified BC-CSRRs, represented by L_c and C_c in the equivalent circuit model, which gives a transmission zero located at:

$$f_{z2} = \frac{1}{2\pi\sqrt{L_c C_c}} \tag{7}$$

In addition, as the rings on the bottom are not united along the common side, the type III structure has a weaker mutual capacitive coupling (C_s) and the frequency of the corresponding transmission zero, f_{z1}, is slightly higher than that of the type II.

For the type IV structure, like the type III there are two transmission zeros. However, whereas that has both transmission zeros in the upper stopband, type IV has one each in the upper and lower stopband, as shown in Fig. 4(c). This is due to the increase of the inductance L_s and the capacitance C_s in the circuit model (see the values of the lumped elements in Table 1). When the rings on the top are aligned back-to-back, the mutual inductive coupling is reduced as they can only receive limited energy though the split. The corresponding inductance L_s thus increases. In the meanwhile, since the two rings on the bottom of type IV structure are aligned back to back, the mutual capacitive coupling is enhanced and thus the corresponding capacitance (C_s) increases. Therefore, the corresponding transmission zero frequency described by (6) also shifts down.

The variation of the orientations of the top rings of the BC-CSRR pairs changes not only the mutual coupling between the BC-CSRR pairs but also the coupling between the SIW and the BC-CSRR. As shown in

Table 1, the value of C_c increased from type type-II to type-IV unit cells by a most significant factor of 7. This is due to the increase of capacitive coupling between the SIW and the BC-CSRR. As we know, the electric field of the CSRR is mainly distributed around the ring and reaches its maximum in the vicinity of the slot opposite to the split of the ring. When the orientations of the top layer rings of the BC-CSRR change from face-to-face to back-to-back (i.e., from type-II to type-IV unit cells), the capacitive coupling between the SIW and the BC-CSRR becomes easier as the slot opposite to the split of the top ring, where the electric field is maximum, is close to the center. Therefore, the corresponding capacitance (C_c) increases.

4. Bandpass Filters with the Proposed New Structures

To design SIW filters based on the proposed BC-CSRR resonator pairs with a required specification, it is important to employ the classic filter design methodology. The design procedure of SIW filters with EC-CSRRs was described in [11]. Generally, it involves three steps: the first step is to use circuit synthesis to get proper design parameters of the filters including the coupling coefficients and external Q factor. Then, even- and odd-mode theory can be employed to analyse the coupling between the resonators. The coupling coefficients can be obtained using [19]:

$$M = \frac{f_1^2 - f_2^2}{f_1^2 + f_2^2} \tag{8}$$

where f_1 and f_2 represent the resonance frequencies of low and high modes, respectively. The external Q factor can be extracted by using a doubly-loaded resonator and calculated by [19]:

$$Q_e = \frac{2 f_0}{\Delta f_{3dB}} \tag{9}$$

where f_0 is the frequency where S_{21} is maximum; Δf_{3dB} denotes the 3-dB bandwidth for which S_{21} is reduced by 3 dB from the maximum value. After this step, the relationship between the coupling coefficients and the physical structures of coupled resonators can be established to obtain the physical configuration of the required filter. Finally, optimisation is carried out as usual to get the best possible result. In this section, bandpass filters using the Type I, II, III, IV cells are designed and optimized using HFSS™. They are based on resonators coupled by an evanescent-mode waveguide section. The filters were fabricated using a standard PCB etching process and measured with an Agilent E8363A network analyzer.

4.1 Type I Bandpass Filter

With the previously mentioned method, a second-order bandpass filter based on the type I unit cell (see Fig. 1) was designed and optimised with HFSS™. The layout of the filter is presented in Fig. 5(a), where two identical BC-CSRR pairs are employed and coupled with an evanescent-mode waveguide section. The center frequency of the filter can be tuned by changing the length of the BC-CSRR (b), the width of the slot (d) and the width of the gap (g). The decrease of d and g, or the increase of b could lead to a lower center frequency. The bandwidth

of the filter can be adjusted by varying the length of the evanescent-mode SIW section (ld). A larger ld could lead to a weaker coupling and a narrower bandwidth as shown in Fig. 2(b). In addition, the parameters of the transition, namely, the length (ys) and width (ws) of the slot of the transition, can be adjusted to achieve a better match between the BC-CSRR and the input microstrip. However, it should be noted that, the variation of the width of the SIW (w) can also influence the filter response. As shown in the following Fig. 7, the bandwidth of the filter is widened with the increase of w. This is due to the increase of coupling between resonators with increase of w. When w increases, the cutoff wavelength of the waveguide (λ_c) is lowered, therefore, the evanescent-mode coupling between resonators is enhanced and hence the bandwidth is widened [20].

A prototype of the filter based on the type I unit cell was fabricated. The filter was fabricated on the dielectric substrate FB4-1/2 with ε_r = 2.65 and thickness of 1 mm. Fig. 6(a) show a photograph of the fabricated filter. The size of the filter, excluding feed-lines, is 20 mm × 13 mm. Detailed dimensions of the filter are given in Table 2. Fig. 8(a) shows the simulated and measured frequency response of the filter over the 4.5 to 7.5 GHz band, with a measured centre frequency and 3 dB bandwidth of 5.75 and 0.3 GHz, respectively. The in-band return loss is better than 12 dB and the insertion loss is 4 dB including the microstrip feed lines and SMA connectors [6].

4.2 Bandpass Filters with Type II, III and IV Unit Cells

Second-order SIW bandpass filters with the type II (as per Fig. 3(a)), type III (see Fig. 3(b)) and type IV (see Fig. 3(c)) unit cells were designed and optimized with HFSS™ following similar procedures to the design and optimization of the filter with type I unit cells. These filters were fabricated on Rogers 4350 substrate with ε_r = 3.48 and thickness of 0.762 mm. Fig. 5(b)-(d) and Fig. 6(b)-(d) show the layouts and the photographs of the filters based on these three new types of unit cell, with detailed dimensions provided in Table 2. The simulated and measured transmission responses of the SIW filters are presented in Fig. 7(b)-(d).

Fig. 8(b) presents the simulated and measured transmission responses of the SIW filters based on the type II unit cell. The measured centre frequency and 3 dB bandwidth of the fabricated filter are 4.43 and 0.69 GHz, respectively. The measured insertion loss is approximately 1.4 dB including the feed lines and SMA connectors. A transmission zero located in the upper band is observed. Due to the existence of the transmission zero, the measured stopband rejection is better than 25 dB from 5.06 GHz to 7.5 GHz.

Fig. 8(c) shows the simulated and measured transmission responses of the filter based on the type III over the 3 to 9.25 GHz band. It can be seen that the measured centre frequency and 3 dB bandwidth are 5.15 and 0.85 GHz, respectively. The measured insertion loss is approximately 1.1 dB including the feed lines and SMA connectors. Moreover, two transmission zeros located in the upper band are also obtained. The measured stopband rejection from 5.73 GHz to 9 GHz is better than 20 dB.

The simulated and measured transmission responses of the filter with the type IV unit cell over the 3 to 6.5 GHz band are depicted in Fig. 8(c). The measured center frequency and 3 dB bandwidth are 5.1 and 0.37 GHz, respectively. The measured insertion loss is approximately 4dB including the feed lines and SMA connectors. It

can be seen that the measured loss of type IV filter is higher than that of the type II and type III filters. This might result from the narrow bandwidth of the filter. Since the bandwidth of the type IV filter is much narrower than that of the type II and type III filters, the length of the evanescent-mode SIW section (ld) of type IV filters needs to be much longer than that of the type II and type III filters in order to achieve a weaker coupling. From Table 2, it can be seen that the value of ld for the type I and type IV filters is indeed much larger than that of the type II and type III filters. The increase of ld could lead to a higher dielectric loss and conductor loss, therefore, the type IV filter shows a higher insertion loss than that of the type II and type III filters. However, for the type IV filter, transmission zeros located both in the upper and lower stopband have achieved. Therefore, compared with the previous three types of filters, it shows improved selectivity.

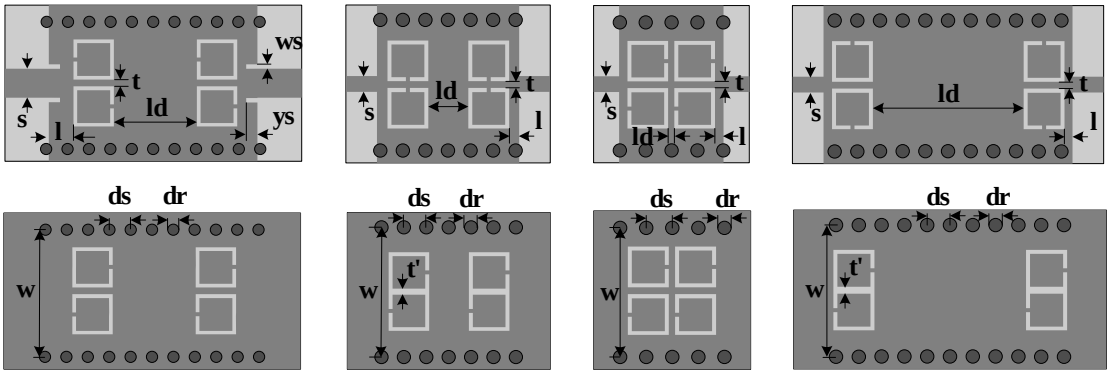

(a) (b) (c) (d)

Fig. 5. Layout of the filters base on: (a) type I unit cells (see the first column), (b) type II unit cells (see the second column), (c) type III unit cells (see the third column) and (d) type IV unit cells (see the forth column).

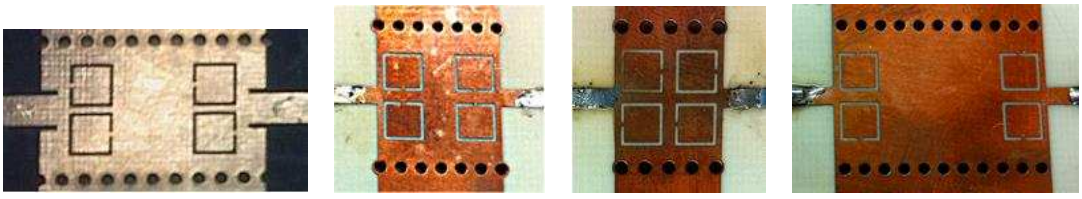

(a) (b) (c) (d)

Fig. 6. Top view of the photograph of the fabricated filters base on: (a) type I unit cells, (b) type II unit cells, (c) type III unit cells and (d) type IV unit cells.

Table 2. Parameters of the filters base on the type I, type II, type III and type IV unit cells (unit: mm)

	b	g	d	t	w	s	l	dr	ds	ld	t’	ws	ys
Type I	3.9	0.3	0.34	0.5	12.5	2.65	2.5	1.1	2	7	-	0.5	1.5
Type Ⅱ	3.9	0.3	0.34	1.1	14.5	1.68	0.5	1.1	1.9	3	0.43	-	-
Type Ⅲ	3.9	0.3	0.34	0.8	12.5	1.68	0.5	1.2	2.2	1.1	-	-	-
Type Ⅳ	3.9	0.3	0.34	1.1	14.5	1.68	0.5	1.1	1.9	12	0.33	-	-

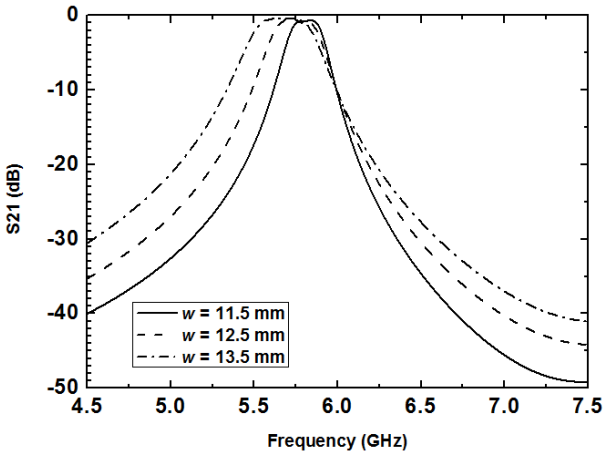

Fig. 7 Simulated S21 of the SIW filter based on the type I unit cell with different width of the waveguide (w).

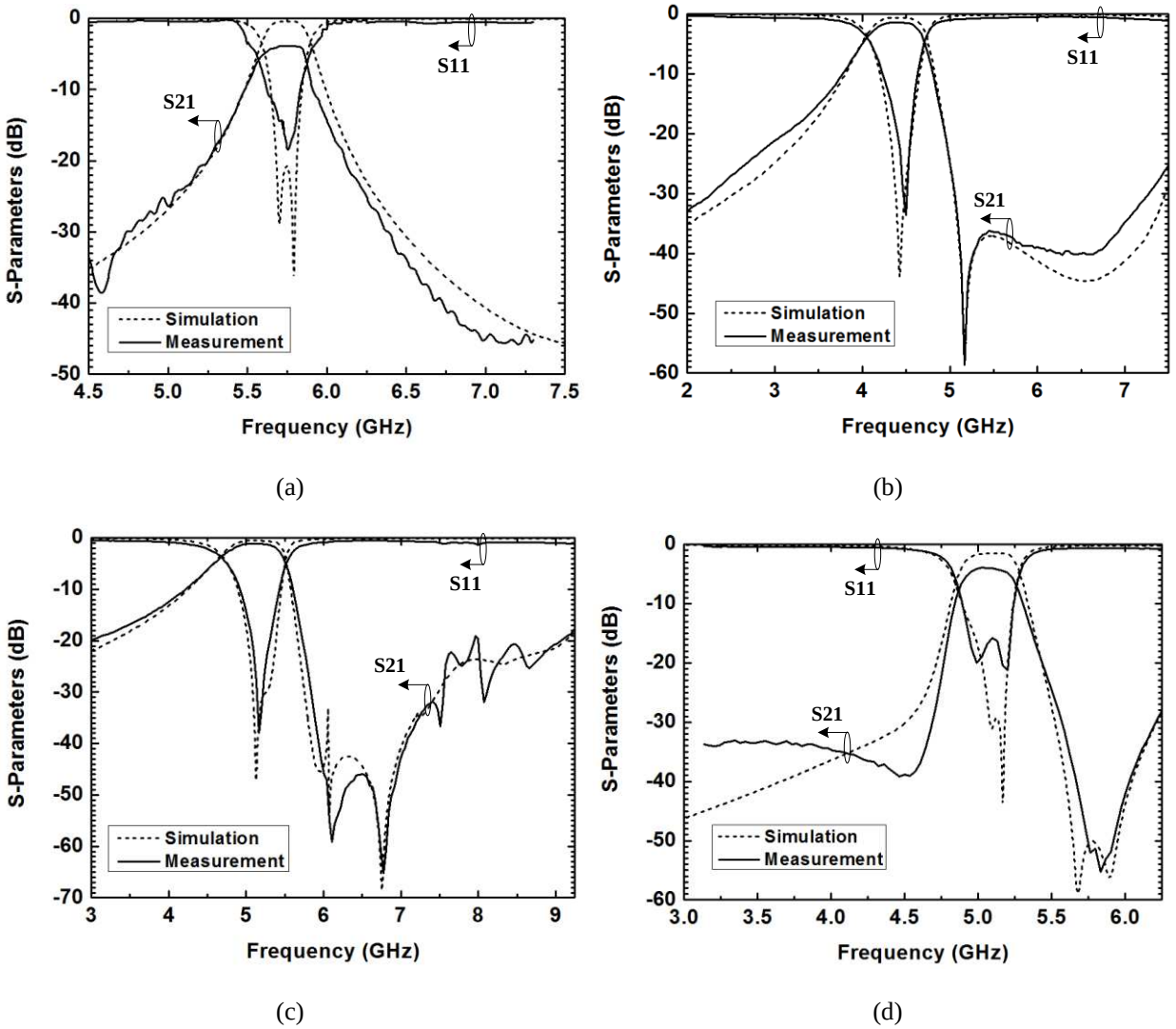

Fig. 8. Simulated and measured frequency responses of the filters base on: (a) type I unit cells, (b) type II unit cells, (c) type III unit cells and (d) type IV unit cells.

5. Conclusions

Novel band-pass substrate integrated waveguide (SIW) filters based on broadside-coupled complementary split ring resonator (BC-CSRR) and modified BC-CSRR resonator pairs have been described. The centre frequency of the proposed filters is located below the cutoff frequency of the waveguide. Four SIW-BC-CSRR resonator structures have been introduced and compared by changing the orientation of the rings on the upper broadwall. Based on these resonators, bandpass filters have been designed and fabricated. It is shown that these filters are compact and easy to fabricate and integrate with other electric circuits and they have great potential for low-cost integrated microwave circuits. The type IV unit cell provides two poles and two zeroes, one above and one below the centre frequency, and this gives considerable advantage for the design of a miniature filter with high performance.

References

[1] D. Deslandes, and K. Wu, "Single-substrate integration technique of planar circuits and waveguide filters," IEEE Trans. Microw. Theory Tech., vol. 51, no. 2, pp. 593-596, Feb. 2003.

[2] W. Che, C. Li, K. Deng, and L. Yang, "A novel bandpass filter based on complementary split rings resonators and substrate integrated waveguide," Microw. Opt. Technol. Lett., vol. 50, no. 3, pp. 699-701, Nov. 2008.

[3] J. B. Pendry, A. J. Holden, D. J. Robbins, and W. J. Stewart, "Magnetism from conductors and enhanced nonlinear phenomena," IEEE Trans. Microw. Theory Tech., vol. 47, no. 11, pp. 2075-2084, Nov. 1999.

[4] R. Marque´s, F. Medina, and R. Rafii-El-Idrissi, "Role of bianisotropy in negative permeability and left-handed metamaterials," Phys. Rev. B, , vol. 65, 144440, Apr. 2002.

[5] F. Falcone, T. Lopetegi, J. D.Baena, R. Marqués, F. Martín, and M. Sorolla, "Effective negative-ε stopband microstrip lines based on complementary split ring resonators," IEEE Microw. Wireless Compon. Lett., vol. 14, no. 6, pp. 280-282, Jun. 2004.

[6] L. Huang, I. D. Robertson, N. Chang, and J. Huang, "Novel substrate integrated waveguide bandpass filter with broadside-coupled complementary split ring resonators," 2012 IEEE MTT-S Int. Microw. Symp. Dig.

[7] R. Marqués, F. Mesa, J. Martel, and F. Medina, "Comparative analysis of edge-and broadside-coupled split ring resonators for metamaterial design—theory and experiments," IEEE Trans. Antennas Propag., vol. 51, no.10, pp. 2572-2581, Oct. 2003.

[8] J. D. Baena, J. Bonache, F. Martin, R. Marques, F. Falcone, T. Lopetegi, M. A. G. Laso, J. Garcia, I. Gil, and M. Sorolla, "Equivalent-circuit models for split-ring resonators and complementary split-ring resonators coupled to planar transmission lines," IEEE Trans. Microw. Theory Tech. , vol. 53, no. 4, pp. 1451-1461, Apr. 2005.

[9] H. X. Xu, G. M. Wang, C. X. Zhang, Z. W. Yu, and X. Chen, "Composite right/left-handed transmission line based on complementary single-split ring resonator pair and compact power dividers application using fractal geometry," IET Microw. Antennas Propag., vol. 6, pp. 1017-1025, Jun. 2012.

[10] X. P. Chen, and K. Wu, "Substrate integrated waveguide cross-coupled filter with negative coupling structure," IEEE Trans. Microw. Theory Tech., vol. 56, pp. 142-149, Jan 2008.

[11] Y. D. Dong, T. Yang, and T. Itoh, "Substrate integrated waveguide loaded by complementary split-ring resonators and its applications to miniaturized waveguide filters," IEEE Trans. Microw. Theory Tech. , vol. 57, no. 9, pp. 2211-2223, Sep. 2009.

[12] C. Li, and F. Li, "Microstrip bandpass filters based on zeroth-order resonators with complementary split ring resonators," IET Microw. Antennas Propag., vol. 3, pp. 276-280, Mar. 2009.

[13] J. Bonache, M. Gil, I. Gil, J. Garcia-Garcia, and F. Martin, "On the electrical characteristics of complementary metamaterial resonators," IEEE Microw. Wireless. Compon. Lett., vol. 16, pp. 543-545, Oct. 2006.

[14] D. M. Pozar, "Microwave Engineering. Reading," vol. MA: Addison-Wesley, 1990.

[15] J. Esteban, C. Camacho-Peñalosa, J. E. Page, T. M. Martín-Guerrero, and E. Márquez-Segura, "Simulation of negative permittivity and negative permeability by means of evanescent waveguide modes—theory and experiment," IEEE Trans. Microw. Theory Tech., vol. 53, no. 4, pp. 1506-1514, Apr. 2005.

[16] P. Belov, and C. Simovski, "Subwavelength metallic waveguides loaded by uniaxial resonant scatterers," Phys. Rev. E, Stat. Phys. Plasmas Fluids Relat. Interdiscip. Top., vol. 72, pp. 0366181-03661811, Sep. 2005.

[17] V. Radonić, V. Crnojević-Bengin, and B. Jokanović, "On the orientation of split-ring resonators in metamaterial media," 8th International Conference on Telecommunications in Modern Satellite, Cable and Broadcasting Services pp. 645 - 648, 2007

[18] F. Hesmer, "Coupling mechanisms for split ring resonators: theory and experiment," Phy. Stat. Sol. (b), vol. 224, no. 4, pp. 1170-1175, Mar. 2007.

[19] J. G. Hong, and M. J. Lancaster, "Microstrip filters for RF/microwave applications," New York: John Wiley & Sons, 2001.

[20] G. F. Craven, and C. K. Mok, "The design of evanescent mode waveguide bandpass filters for a prescribed insertion loss characteristic," IEEE Trans. Microwave Theory Tech vol. 19, pp. 295 - 308 1971.